frontiers in Photobiology

TYPE Methods
PUBLISHED 28 May 2026
DOI 10.3389/fphbi.2026.1800988

OPEN ACCESS

EDITED BY
Matteo Di Giosia,
University of Bologna, Italy

REVIEWED BY
Leander Rohr,
University of Tübingen, Germany
Marco Malferrari,
University of Bologna, Italy

*CORRESPONDENCE
Anna Bosc,
anna.bosc@polimi.it
Giuseppe Maria Paternò,
giuseppemaria.paterno@polimi.it

RECEIVED 31 January 2026
REVISED 29 April 2026
ACCEPTED 05 May 2026
PUBLISHED 28 May 2026

CITATION
Bosc A, Pianetti A and Paternò GM (2026) Quantifying motility-based biological responses in Chlamydomonas reinhardtii using an integrated single-cell framework. *Front. Photobiol.* 4:1800988. doi: 10.3389/fphbi.2026.1800988

Quantifying motility-based biological responses in Chlamydomonas reinhardtii using an integrated single-cell framework

Anna Bosc[1,2]*, Andrea Pianetti[2] and Giuseppe Maria Paternò[1,2]*

[1]Politecnico di Milano, Department of Physics, Milano, Italy, [2]Istituto Italiano di Tecnologia, Center for Nano Science and Technology, Milano, Italy

Quantitative monitoring of motility in biological microswimmers is an essential instrument for understanding how microorganisms perceive, process, and translate external stimuli into dynamic behavioural responses. However, tactical responses emerge from complex biophysical mechanisms that operate simultaneously at the individual and collective levels, giving rise to intra-population heterogeneity that can be difficult to quantify with population-averaged approaches: when the trajectories of kinematically distinct subgroups are aggregated, coherent responses may appear weak or confused even in the presence of organised subpopulations. In this work, we present a single-cell tracking-based method for the rigorous kinematic characterisation of the phototactic response of *Chlamydomonas reinhardtii*, with the aim of resolving behavioural variability and its temporal evolution within heterogeneous populations. The workflow integrates automated large-scale tracking, detailed trajectory reconstruction, single-cell and population-level kinematic analysis, segmentation into coherent behavioural subpopulations (stationary, confined/circling, and directional) via clustering in circular feature space, and characterisation of dynamic motion regimes through time-windowed mean squared displacement (MSD) analysis. By explicitly decomposing the population into coherent kinematic components and quantifying their relative contributions, the method provides "behavioural resolution" of mixed phototactic responses. Based exclusively on open-source software and robust mathematical analysis, the method is highly reproducible and easily extendable to the study of other biological or synthetic microswimmers subjected to controlled external stimuli.

KEYWORDS
behavioural analysis, Chlamydomonas reinhardtii, kinematic analysis, microswimmers, phototaxis, single-cell tracking

1 Introduction

Quantitative monitoring of motility in biological microswimmers is a powerful and reproducible approach for investigating how microorganisms perceive and integrate external stimuli, and how these stimuli modulate their behavioural dynamics over time. Tactical responses, namely, the active reorientations of swimming direction guided by physical or chemical signals, emerge from the interaction between sensory perception, intracellular transduction, and motility regulation (Tsang and Riedel-Kruse, 2024; Wang

and Tsang, 2025). These processes operate on remarkably different timescales, ranging from milliseconds to tens of minutes. Sagawa et al. (2014) demonstrated that enzymatic reactions in bacterial chemotaxis take approximately 240 milliseconds, while Korobkova et al. (Korobkova et al., 2004) showed that behavioural changes occur on timescales ranging from a few seconds to several minutes.

Phototaxis is a paradigmatic example of such active responses, enabling mobile microorganisms such as microalgae and cyanobacteria to detect and orient themselves in light gradients. Light adaptation acts as an "oscillatory dampener" that mediates responses on subcellular (flagellar beating), cellular (phototaxis), and population (pattern formation) scales, covering time scales from milliseconds to 30 min (Wang and Tsang, 2025).

Individual cells can respond to light changes within minutes (Chau et al., 2015), and a simple "photoresponse reversal mechanism" allows them to switch from one flagellar beating state to another, generating different behavioural responses (Tsang and Riedel-Kruse, 2024), demonstrating what Irimia (2010) described as "slower and faster signalling events occurring simultaneously within moving cells." Taken together, these studies illustrate how microswimmers dynamically integrate sensory perception across different timescales through sophisticated adaptive feedback mechanisms.

In addition to its physiological importance for individual cells, phototaxis plays a key role in the ecology of aquatic environments and in the performance of photobioreactors. The response can be modulated by physical factors, such as light intensity (Chau et al., 2015; Feinleib and Curry, 1971), fluid viscosity (Drescher et al., 2010), chemical factors such as extracellular Ca^{2+} concentration (Morel-Laurens, 1987), and intrinsic factors such as cell density, because even when individual cells can respond to light independently, colonies move collectively, highlighting the interaction between individual and collective effects (Varuni et al., 2017; Choudhary et al., 2019).

Although the biophysical mechanisms of phototaxis have been elucidated by detailed physical models, such approaches, often analytical or based on single cells, capture only part of the complexity. Numerous subsequent studies (Leptos et al., 2013; Polin et al., 2009) have highlighted the stochastic nature of the swimming pattern and the coexistence of rectilinear motions and rotational phases. Others have linked the phototactic response to metabolic and redox status (Wakabayashi et al., 2011) or to light history-dependent adaptation (Arrieta et al., 2017), revealing that phototaxis is a dynamic and context-dependent process.

Despite substantial progress in modelling and interpreting phototaxis, experimental analysis methods still tend to emphasise either single-cell mechanistic studies or population-averaged descriptors (e.g., mean velocities or global direction vectors). In heterogeneous samples, however, opposite taxis signs and distinct motility modes can coexist; when trajectories are pooled, these components partially cancel, and the collective response can appear weak or noisy even when coherent subgroups are present. This creates a practical gap: a scalable and reproducible workflow is needed that jointly provides (i) quantification of directionality relative to a defined stimulus axis with appropriate circular statistics, (ii) resolution of intra-population heterogeneity into interpretable behavioural classes, and (iii) characterisation of how dynamical regimes evolve over time after stimulation. Theoretical advances in modelling "intelligent micronavigators" (Colabrese et al., 2025) further underscore the need for a quantitative experimental framework linking individual behaviour and collective responses.

Here we address this gap by introducing an integrated single-cell framework for phototaxis analysis in *Chlamydomonas reinhardtii*. The workflow couples large-scale automated tracking with (i) kinematic segmentation into stationary, confined/circling, and directional behaviours; (ii) identification of stimulus-consistent directional subpopulations via clustering in circular feature space; and (iii) time-windowed MSD analysis with model-based regime classification to capture stimulus-driven transitions that are invisible to global averages. By explicitly decomposing the population into coherent kinematic components and quantifying their relative contributions, the method provides "behavioural resolution" of mixed phototactic responses. Implemented using open-source tracking and shared code/data, the approach is readily transferable to other biological or synthetic microswimmers under controlled external cues.

2 Materials and equipment

2.1 Experimental setup

The experiments were conducted using a fluorescence microscopy system specifically designed for the analysis of motility under stimulation (Figure 1). The setup replicates and modifies the architecture described in Ghezzi et al. (2023).

The excitation illumination comes from a six-wavelength LED source (Chrolis™ Thorlabs). The beam is modulated by a Digital Micromirror Device (DMD, V-7000 ViaLUX GmbH), reflected on a dichroic filter and focused on the sample. The emitted fluorescence follows the same optical path, passes through the dichroic filter and one or more bandpass or long-pass selective filters, and is collected by a scientific CMOS camera (Hamamatsu Orca). The phototactic stimulation system is arranged at 90° to the imaging path and consists of a fibre-coupled LED focused on the edge of the sample to produce a divergent light gradient inside the observed focal plane.

To study the phototaxis of *C. reinhardtii* samples, images were acquired with a ×4 objective. Videos were acquired at a frame rate of 10 fps. Chlorophyll excitation was performed at 625 nm (power on the sample = 28.5 μW) and collected above 680 nm with a long-pass filter, while phototactic stimulation was conducted at 470 nm (power output at the focal point = 123 μW).

2.2 Biological samples

The experiments were conducted using the unicellular green alga *C. reinhardtii* WT124 mt-, grown in TAP (Tris-Acetate-Phosphate) (Gorman and Levine, 1965) liquid medium under gentle agitation at 21 °C. Cultures in exponential growth phase were used for all measurements.

For the swimming and phototaxis tests, the cells were diluted in Minimal Medium (Gorman and Levine, 1965) to an OD of 0.400 ± 0.05, and then loaded into single-channel chambers with a thickness of 200 μm (IBIDI μ-Slide I Luer 0.2 mm), which provide a uniform sample depth and minimise hydrodynamic artifacts during motility analysis.

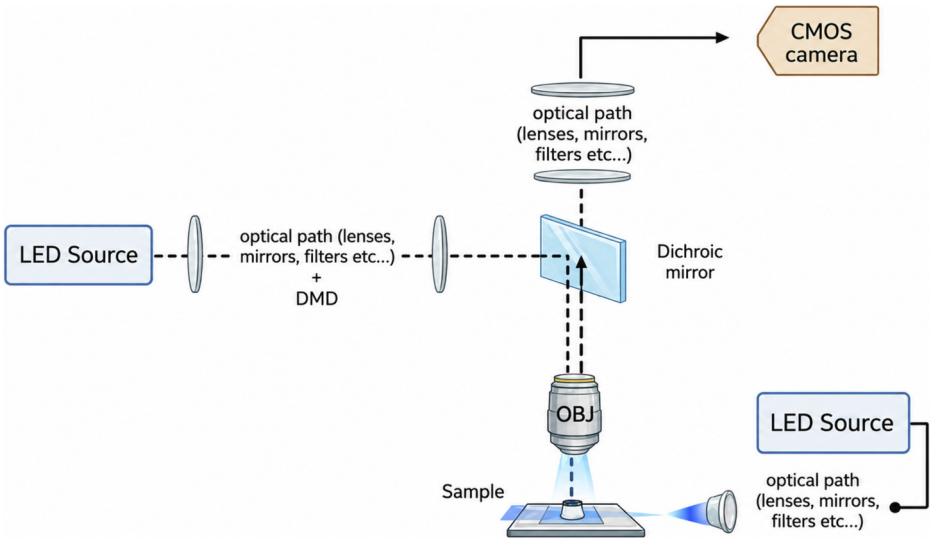

FIGURE 1
Optical scheme of the microscope. The excitation path (left) consists of an LED source followed by a collimating optical path (lenses, mirrors, bandpass filters) and a Digital Micromirror Device (DMD) for spatially structured illumination. The excitation light is directed onto the sample through a dichroic mirror and an objective lens (OBJ). Fluorescence emission is collected by the same objective, separated from the excitation path by the dichroic mirror, and directed through an emission optical path (lenses, mirrors, filters) to a CMOS camera for image acquisition. A second LED source, positioned laterally along the sample plane, provides the directional light stimulus used to elicit phototactic responses.

All experiments were conducted at room temperature.

2.3 Acquisition and tracking software

The fluorescence videos were processed with FIJI-ImageJ (Schneider et al., 2012) using the TrackMate plugin (Ersho et al., 2022), with LoG detection and nearest-neighbour linking. Approximately 400–600 cells were tracked for each video, applying quality and continuity filters to remove spurious trajectories. The method is scalable to larger datasets. The data analysis was conducted with MATLAB (The MathWorks Inc. MATLAB, 2022). The parameters used for Trackmate are reported in the Supplementary Material (SI). For the representative dataset presented in the Results, 607 trajectories were returned by TrackMate at 10 fps.

Each acquisition was limited to 60 s in order to balance temporal resolution and statistical robustness. Given the computational constraint on the maximum number of simultaneously tracked trajectories (~400–600), extending the acquisition time would reduce the temporal density of trajectories, as the same number of tracks would be distributed over a longer time window. This would decrease the number of trajectories available per unit time and reduce the statistical power of the analysis of the phototactic response.

The chosen time window therefore represents a compromise that allows capturing the evolution of the phototactic behaviour while maintaining a sufficiently high number of trajectories. This choice is consistent with the large field of view provided by the ×4 objective, which is optimised for population-level analysis rather than long-term tracking of individual cells. The approach can be extended to longer acquisition times depending on computational resources and experimental conditions.

3 Methods

The coordinates (x, y) of the particles were exported and analysed in MATLAB (The MathWorks Inc. MATLAB, 2022), reconstructing a matrix for each cell that describes its coordinates over time.

3.1 Kinematic parameters of single cells

For each trajectory, the following parameters have been calculated: incremental displacement, instantaneous and average velocity, directional change rate (DCR), track duration, net and total displacement, average direction, directional force (r). The mathematical definitions are shown in Table 1. These parameters constitute the basis for identifying trajectories that are consistent in terms of motility, persistence and orientation, and allow an initial distinction to be made between stationary, confined or directional behaviours.

3.2 Collective kinematic analysis

To characterise the kinematic behaviour of the population as a whole, the parameters of the individual cells are aggregated (Equations reported in Table 2). The statistical significance of the alignment between overall net movement and external stimulus is evaluated using the Rayleigh test (Fisher, 1995). Rayleigh's statistic is obtained by the following equations reported in Table 3, where n is the number of observations.

These components are used to calculate the p-value as shown. The Rayleigh test assesses whether the distribution of angles is random (z small, p large) or directional (z large, p small). The alignment with a generic stimulus of direction $\vec{L}$ is calculated by

10.3389/fphbi.2026.1800988

TABLE 1 Kinetic parameters from trajectories.

Kinetic parameter	Equation
Displacement: Euclidean distance between two consecutives frames	$D_i = \sqrt{\left\{(x_{\{i\}} - x_{\{i-1\}})^2 + (y_{\{i\}} - y_{\{i-1\}})^2\right\}}$
Speed Δt is 1 if we are considering frames, or the time that connects two consecutive frames	$v_i = \frac{D_i}{\Delta t}$
Directional change rate (DCR) DCR represents the direction of movement between two frames. The arctan2 function returns the correct angle in the entire plane	$\theta i = arctan2(y_{j+1} - y_j, x_{j+1} - x_j)$
Track duration: is the number of frames in which the cell track is observed. The formula accounts for the fact that the cell is present in both the start and end frame (hence the +1). Allows filtering out overly short (often spurious) tracks and evaluating tracking stability.	$t_{i,j} = \text{frame}_{end,j} - \text{frame}_{start,i} + 1$
Net displacement: is the Euclidean distance between the start and end point of the track. Indicates how far the cell has actually moved, regardless of the path taken. It is a useful parameter that could be used to distinguish active (high net displacement) from static or poorly motile cells	$d_{i,j} = \sqrt{(x_{end,j} - x_{start,i})^2 + (y_{end,j} - y_{start,i})^2}$
Total displacement (trajectory length) The total displacement is the sum of the distances between all consecutive points on the track. If the cell moves a lot but along convoluted path, Dtot may be much larger than dnet. Measures absolute motility, even in the absence of net migration	$D_{tot} = \sum_{j=1}^{N-1} \sqrt{(x_{\{j+1\}} - x_j)^2 + (y_{\{j+1\}} - y_j)^2}$
Mean velocity of the track The instantaneous velocity is the distance covered in a time interval Δt between two consecutive frames. The mean velocity is the average of the instantaneous velocities over the whole track Allows comparison of motility between cells and between different experimental conditions	$v_{mean}^{track} = \frac{1}{n-1} \sum_{j=1}^{n-1} v_j$
Mean Direction vector (directional strength, *r*) From DCR parameter θ, we can calculate the directional strength r that quantifies the alignment of the population toward a direction Each direction is represented as a unit vector in the plane; their normalised vectorial sum measures global alignment. r = 1 means all directions are equal, r ≈ 0 means they are random	$\langle \cos\theta \rangle = \frac{1}{N} \sum_{j=1}^{N} \cos\theta_j \; ; \; \langle \sin\theta \rangle = \frac{1}{N} \sum_{j=1}^{N} \sin\theta_j$ $r = \sqrt{\langle \cos\theta \rangle^2 + \langle \sin\theta \rangle^2}$

TABLE 2 Definitions of the global net-movement vector obtained by aggregating single-cell displacements: magnitude |R|, angle (θ), and mean direction (θ mean) computed from the summed unit vectors of individual trajectory directions.

Parameter	Equation
Global net movement	$\vec{M}_x = \frac{1}{N} \sum_{i=1}^{N} x_{(end,i)} - x_{(start,i)}$ $\vec{M}_y = \frac{1}{N} \sum_{i=1}^{N} y_{(end,i)} - y_{(start,i)}$ $\vec{M}_{net} = (\vec{M}_x, \vec{M}_y)$
Magnitude	$\lvert\vec{M}_{net}\rvert = \sqrt{M_x^2 + M_y^2}$
Angle	$\theta = arctan2(My, Mx)$
Mean Direction (θmean)	$\theta_{mean} = arctan2(\langle sin\,\theta \rangle, \langle cos\,\theta \rangle)$ $\vec{C} = (\langle cos\,\theta \rangle, \langle sin\,\theta \rangle)$

comparing it with the mean direction of the population, vector $\vec{C}$ (Table 2) as shown in Equations 1, 2. Alignment is +1 if perfectly parallel, 0 if orthogonal, −1 if opposite. This is for measuring the consistency of the response relative to the stimulus orientation.

TABLE 3 Rayleigh test for non-uniformity of angular distributions. Definitions of the resulting vector length, mean resultant length, Rayleigh's statistic (z), and corresponding p-value (including the large-n approximation) used to quantify whether population directions differ from a random uniform distribution.

Parameter	Equation
Resulting vector	$R = \sqrt{(\sum_i cos\,\theta_i)^2 + (\sum_i sin\,\theta_i)^2}$
Mean length	$\bar{R} = \frac{R}{n}$
Rayleigh's statistic	$z = n\bar{R}^2 = \frac{R}{n}^2$
p-value	$p \approx e^{-z}(1 + \frac{2z - z^2}{4n} - \frac{24z - 132z^2 + 76z^3 - 9z^4}{288n^2})$
Approximated p-value for n > 50	$p \approx e^{-z}$

$$\Delta\theta_{stim} = arccos\left(\frac{\vec{C} \cdot \vec{L}}{\left|\vec{C}\right| \left|\vec{L}\right|}\right) \quad (1)$$

$$alignment = cos(\Delta\theta_{stim}) \quad (2)$$

A critical point is that the vectorial sum is strongly penalised by small transversal movements or noise (oscillations, deviations),

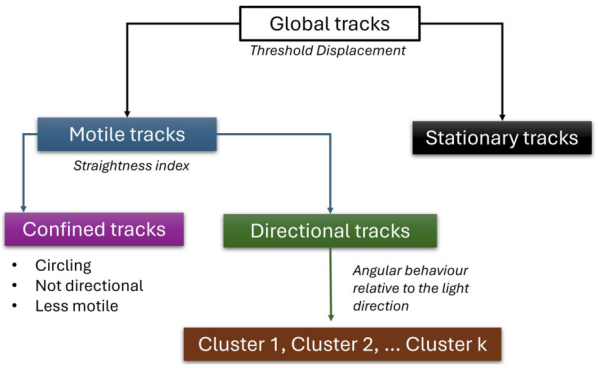

FIGURE 2
Classification workflow for kinematic subpopulation analysis. Schematic overview of the sequential segmentation procedure applied to the full track population. Global tracks are first partitioned into Stationary and Motile subgroups using a net displacement threshold (*d*th). Motile tracks are further divided into Confined/Circling and Directional subgroups using the straightness index (S). Directional tracks are finally clustered into stimulus-consistent subpopulations (Cluster 1, Cluster 2, . . . Cluster k) based on their angular behaviour relative to the light direction, using k-means clustering in circular feature space.

because they mutually compensate each other. This is why subpopulation dynamics remain "hidden" within the noise, making it necessary to extract the kinematic subpopulations, as presented in the following sections, and motivating the need for a structured analysis of intra-population variability.

3.3 Classification of trajectories into kinematic subpopulations

The population of a biological sample such as Chlamydomonas can exhibit considerable heterogeneity in swimming patterns: persistent rectilinear trajectories, confined or orbiting motions, and stationary or highly directional behaviours can coexist. A direct average over the total population can obscure behaviours linked to responses to external stimuli, making them difficult to detect.

To overcome this limitation, we developed a dynamic segmentation procedure based on kinematics, classifying cells into behavioural subpopulations (Stationary/unmotile, Confined/circling, and Directional as schematically illustrated in Figure 2) according to the parameters described above. These parameters define a feature space in which kinematically similar trajectories cluster together. The goal is not to classify cells statically, but to isolate recurring kinematic components that represent distinct behaviours within the population.

Trajectories were first partitioned into *Stationary/unmotile* and *Motile* using a net *threshold displacement dth*. A track was defined as *Motile* if its net displacement d (the straight-line distance between the first and last recorded position) exceeded the threshold (d > *d*th), indicating that the cell underwent sustained translocation rather than remaining confined around an initial position. Cells with d < *d*th were classified as *Stationary/unmotile*, as their net displacement is comparable to positional noise or passive drift rather than active swimming.

Among *motile* tracks, the *straightness index* (see Table 4) was then applied to distinguish *Confined/circling* trajectories (S < 0.3) from *Directional* ones (S > 0.3). S ranges from 0 to 1, where values close to 0 indicate highly convoluted or looping paths and values close to one indicate trajectories that closely follow a straight line.

Both displacement and straightness thresholds were determined through an empirical calibration procedure, following the same rationale. For *d*th, net displacement values were estimated on representative tracks across multiple samples by measuring the straight-line distance between first and last position in TrackMate. For S, straightness values were estimated on the representative tracks by measuring total path length and applying the formula directly. In both cases, the thresholds were chosen to reflect a meaningful separation between kinematic regimes as observed in the data, and then fixed uniformly across all experimental conditions to ensure cross-dataset comparability.

The distributions of net displacement (Figure 3C) and straightness (Figure 3D) of the full track population serve as post-hoc visual validation of these choices. Both thresholds fall in regions that meaningfully separate distinct kinematic groups: *d*th sits on the descending shoulder of the displacement distribution, distinguishing low-displacement cells from the actively swimming population, while S = 0.3 separates the high-density region of confined low-S tracks from the broader tail of directional trajectories. Importantly, these distributions also illustrate that threshold values are inherently context-dependent: the specific motility patterns of Chlamydomonas, characterised by smooth helical or circular swimming with intermittent reorientations, rather than the sharp tumble behaviour of flagellated bacteria, produce characteristic S distributions that informed our calibration. The classification was further verified by visual inspection of individual traces near the boundary regions of both thresholds.

3.4 Extraction of behavioural subpopulations

Once the kinematic regimes have been identified, clustering algorithms can be applied to detect subpopulations expressing a particular behaviour within each kinematic group. The k-means method, widely used for its simplicity and efficiency, groups cell trajectories into distinct clusters based on quantitative parameters such as speed, direction, or diffusivity, facilitating the understanding of the biological mechanisms underlying behavioural diversity. Here, the algorithm is applied to the angular components (cos θ, sin θ) of directional tracks, allowing clustering in circular feature space (see SI for details). Analysis of the resulting clusters offers a clear perspective on migration strategies and cellular responses to environmental stimuli, revealing the presence of subpopulations with distinct directional behaviour and motility levels. Each subpopulation can then be analysed individually using the kinematic parameters defined above (Table 1 for single-cell kinematics; Tables 2, 3 for mean cluster magnitude, angle, direction, and Rayleigh's statistic).

3.5 Mean squared displacement (MSD) analysis

In the context of characterising cell behaviour, the mean square displacement (MSD) is a fundamental parameter capable of

TABLE 4 Straightness index definition.

Definition	Equations
Straightness index Straightness is a common metric used to quantify how closely a movement follows a straight line. It is defined by the ratio between the total net displacement d_(i,j) that is the Euclidean distance between the start and end of the track (as shown before), and the total distance travelled L (sum of distances between consecutive points)	$d_{i,j} = \sqrt{(x_{end,j} - x_{start,i})^2 + (y_{end,j} - y_{start,i})^2}$ $D_{tot} = \sum_{j=1}^{N-1} \sqrt{(x_{\{j+1\}} - x_j)^2 + (y_{\{j+1\}} - y_j)^2}$ $S = \frac{d_{i,j}}{D_{tot}} = \frac{\sqrt{(x_{end,j} - x_{start,i})^2 + (y_{end,j} - y_{start,i})^2}}{\sum_{j=1}^{N-1} \sqrt{(x_{\{j+1\}} - x_j)^2 + (y_{\{j+1\}} - y_j)^2}}$

aggregating kinetic information into an overview that allows us to describe how cells explore space over time (cell dynamics) and to classify populations into motion regimes. Unlike instantaneous kinetic parameters, MSD measures the effectiveness with which cells move through space, and has been widely applied to characterise the motility of both biological and synthetic microswimmers (Wu and Libchaber, 2000; Urso et al., 2021; Oral et al., 2022; Orozco et al., 2014). MSD is calculated as the mean square distance travelled by a particle as a function of time interval τ. For a single trajectory, MSD is defined in Equation 3, following the standard formalism of single particle tracking and random-walk analysis in biological systems (Qian et al., 1991; Berg, 1993).

$$MSD_\tau = \langle [x(t+\tau) - x(t)]^2 + [y(t+\tau) - y(t)]^2 \rangle \quad (3)$$

MSD is the average over all trajectories of all possible pairs (t, t+τ), where x(t), y(t) are the coordinates at time t, and τ is the lag time between two observations.

Starting from the complete set of particle trajectories, the experiment is divided into short time windows (e.g., 20 frames) to analyse the evolution of behaviour over time. For each time window, the complete trajectories within the interval are extracted, the MSD of each particle is calculated, and finally the mean and standard deviation of the MSD are calculated over all traces in the time window. MSD provides insight into the nature of motion and can highlight transitions from active to passive motion (and *vice versa*), responses to stimuli (e.g., light), metabolic or behavioural changes (e.g., chemotaxis), or interactions with other microorganisms or obstacles (Till et al., 2022).

Analysis of the average MSD function for characterising motion dynamics:

For each time window, the MSD of the *i-particle* is calculated as shown in Equation 4, where x, y (t) is the position of particle i at time t, N is the length of the trajectory, and Δt is the time lag. For each time lag Δt the average MSD is calculated over all particles in the window where M is the number of trajectories in the window (Equation 5) (Qian et al., 1991; Berg, 1993).

$$MSD_i(\Delta t) = \frac{1}{N - \Delta t} \sum_{t=1}^{N-\Delta t} \left([x(t+\Delta t) - x(t)]^2 + [y(t+\Delta t) - y(t)]^2 \right) \quad (4)$$

MSD in time window

$$\langle MSD(\Delta t) \rangle = \frac{1}{M} \sum_{i=1}^{M} MSD_i(\Delta t) \quad (5)$$

MSD in time lag.

By overlaying the MSD curves obtained from the different windows, it is possible to evaluate: the stability of the dynamic regime over time, the arising of direct responses to light stimuli, variations in the persistence of motion or in the mobility of the population.

To quantify the dynamics, the MSD curves are fitted with dynamical models representative of the different types of motion. The fitting allows the extraction of characteristic parameters such as the diffusion coefficient D, the anomalous diffusion exponent α, or confinement scales. Examples of models are reported in Table 5. Qian et al. (1991), Berg (1993). The most appropriate model is selected using linear or non-linear regressions, using R^2, RMSE and parameter confidence intervals as quality criteria.

3.6 Time-dependent motility analysis

The average motility over time was evaluated by calculating the average MSD integrated over all time lags for each window, which provides a summary index of overall motility over time (Equation 6).

$$\overline{MSD}_{window} = \frac{1}{M} \sum_{i=1}^{M} \left[\frac{1}{\Delta t_{max}} \sum_{\Delta t=1}^{\Delta t_{max}} MSD_i(\Delta t) \right] \quad (6)$$

Average integrated MSD.

The time profile of $\bar{MSD}_{window}$ provides a direct measure of the dynamic evolution of the system, facilitating the identification of: variations induced by light stimulation, changes in dynamic regime, interactions and collective phenomena, reduction or increase in subpopulation mobility.

4 Results

To demonstrate the effectiveness of the method developed, we report the analysis of a representative dataset, consisting of a sample with heterogeneous behaviour of *C. reinhardtii*. The experiment consists of acquiring a 60-s video at 10 fps in fluorescence, as follows: 10 s of unperturbed phase in which the cells swim freely, followed by the switching on of an LED (470 nm) that generates a horizontal light gradient within the sample. This configuration generates a heterogeneous phototactic response within the sample, in which subpopulations show positive or negative phototaxis, or local or damped motility in the absence of a phototactic response. A video of the experiment

10.3389/fphbi.2026.1800988

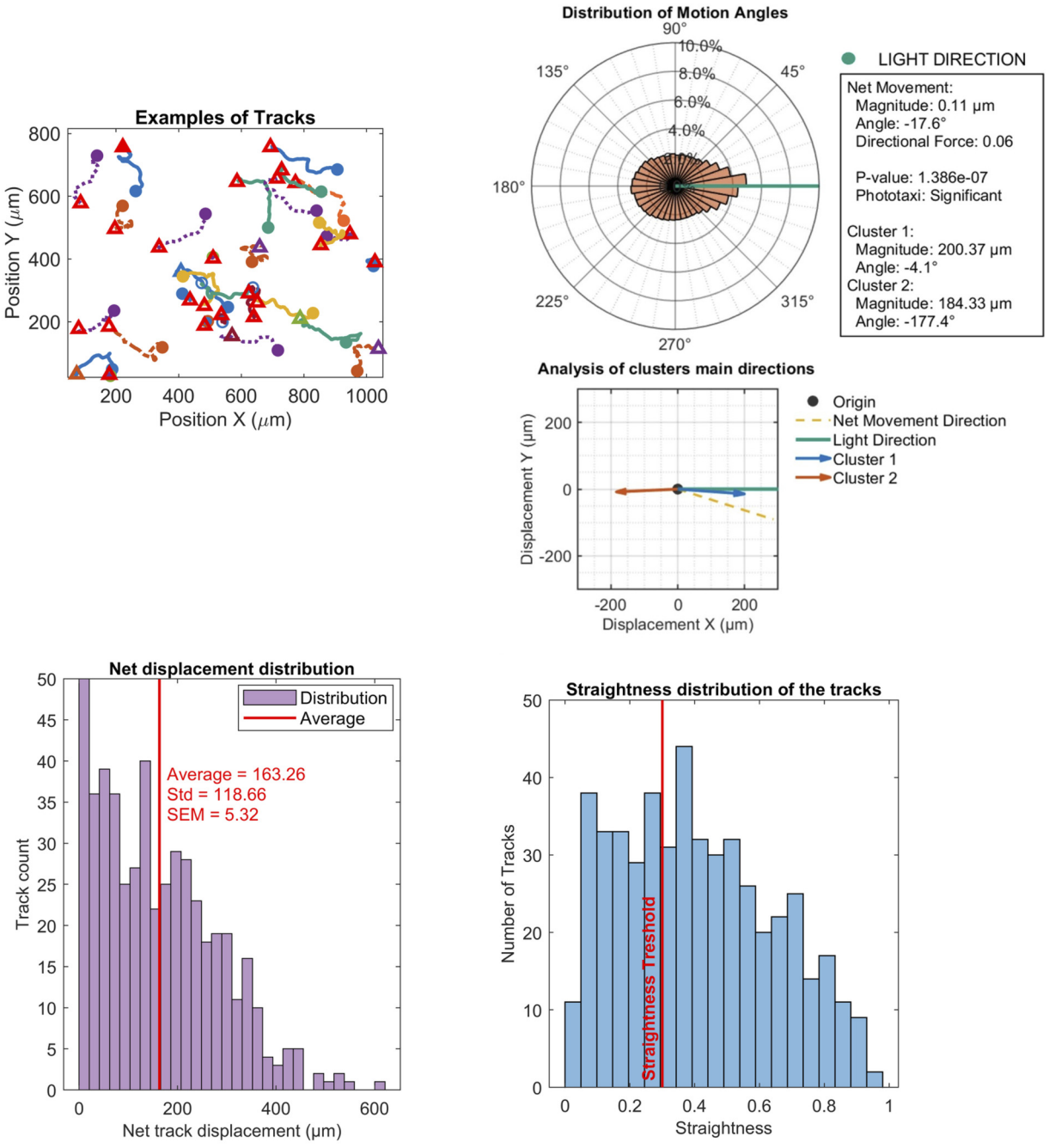

FIGURE 3
Kinematic characterisation of the global population. **(A)** Example of raw cell trajectories traced in the absence of phototaxis. The starting point of the trajectory is marked by a dot, the end by triangle. The high heterogeneity of behavioural patterns highlights the need for structured classification to isolate components of interest. **(B)** Polar histogram and analysis of the distribution of movement angles of the entire population. The absence of a dominant peak confirms the mixed nature of the sample and highlights that the preferred direction occurs only in some subgroups isolated by clustering. The angular parameters of the trajectories are used to divide them into directional subpopulations using k-means. Two distinct clusters emerge, with opposite phototaxis signs. **(C)** Distribution of Net Displacement and **(D)** distribution of rectilinearity of the entire population. The threshold values indicated are those used to distinguish between directional movements and confined/circling movements.

and graphs characterising each subpopulation are provided in the SI.

For the representative dataset presented here, TrackMate returned 607 trajectories. Of these, 497 passed the consistency checks of the tracking reconstruction stage and were retained for the full kinematic analysis.

The complete analyses of three independent biological replicates acquired under identical experimental conditions (same strain, OD = 0.400 ± 0.05, same acquisition and stimulation protocol) are publicly available on Zenodo https://doi.org/10.5281/zenodo.19354253, and their cross-replicate comparison is presented in Supplementary Figure S13 of the Supplementary Material.

TABLE 5 Candidate dynamical models used to fit mean squared displacement (MSD) curves. Analytical MSD expressions and interpretation for Brownian diffusion, ballistic motion, anomalous diffusion/power-law behaviour, polynomial mixed-motion fits, exponential growth/acceleration, exponential confinement (saturation), and Ornstein–Uhlenbeck (harmonic confinement) dynamics; fitted parameters are used to classify motion regimes.

Dynamical models	Equation
Free diffusion (Brownian motion): In the case of pure random motion (such as Brownian motion of particles), the curve will be a straight line, with D is the diffusion coefficient. This linear trend indicates a stochastic motion with no directionality and no acceleration	$MSD(\tau) \sim 4D\tau$
Ballistic motion: Where v represents the constant velocity of the particle. This model describes systems in which motion is oriented and not subject to random changes in direction.	$MSD(\tau) \sim v^2\tau^2$
Anomalous diffusion In cases where movement is hindered or facilitated (e.g., confinement or active motility), the curve follows a power law: $\alpha < 1$ subdiffusive motion, $\alpha > 1$ superdiffusive motion	$MSD(\tau) \sim \tau^{\alpha}$
Polynomial fit (mixed motion) Used for highly variable data or mixed behaviours. As polynomials, they can fit the data well but require caution in interpretation. The coefficient a can be associated with the diffusion coefficient	$MSD(x) = a \cdot x + b$ $MSD(x) = a \cdot x^2 + b \cdot x + c$ $MSD(x) = a \cdot x^3 + b \cdot x^2 + c \cdot x + d$
Exponential type 1 (accelerated motion) Model suitable for describing acceleration dynamics or rapid growth of MSD, typical of activated systems or transient processes	$MSD(x) = a \cdot e^{bx}$
Exponential type 2 (confined motion) Describes the saturation dynamics of MSD, typical of confined systems or particles moving within a limited volume. The curve tends towards a maximum value proportional to the size of the confinement region	$MSD(x) = a \cdot (1 - e^{bx})$
Power law A general model for anomalous diffusion. The exponent b describes the type of behaviour: $b < 1$: subdiffusion (e.g., Confinement, obstacles). $b = 1$: normal diffusion $b > 1$: superdiffusion (persistent active motion)	$MSD(x) = a \cdot x^b$
Ornstein–Uhlenbeck (harmonic confinement): Where $L^2 = 2D\tau_c$ represent the confinement scale and τ_c the characteristic relaxation time. The model describes processes with a force pulling towards a mean position (orbital motion, active confinement).	$MSD(x) = L^2(1 - e^{-\frac{\Delta t}{\tau_c}})$

4.1 Population composition and motion classification

The population is initially characterised as a whole through global kinematic parameters such as average speed, net displacement, directional force (r) (defined in Section 3.1; Table 1) and alignment with the stimulus (Section 3.2), as shown in Figure 3. Based on the Straightness index S and the threshold displacement *d*th (Section 3.3), the population is divided into three kinematic categories: (i) Stationary or unmotile, with local or strictly confined motility; (ii) Confined/circling, characterised by recursive or orbital trajectories; (iii) Directional, i.e., cells that travel along straight/sinusoidal trajectories over long distances. This classification provides a first level of segmentation, which is essential for isolating trajectories representative of light-driven behaviour. K-means clustering is then applied to the directional trajectories, resulting in two distinct subgroups that show a consistent response to the stimulus (positive and negative phototaxis). This segmentation reveals that the mixed population is composed of kinematically heterogeneous but internally consistent subcomponents.

4.2 Characterisation of subpopulations

All subpopulations (stationary, circling, and directional clusters) were analysed and characterised individually. Comparison between them shows marked differences in terms of average orientation, angular distribution, mean speed, and net displacement, confirming the method's ability to effectively disaggregate functionally distinct subpopulations. The individual analyses of the subgroups are presented in the SI.

To statistically validate the separation between subgroups, a Kruskal–Wallis test was applied to the mean swimming speed across the four subpopulations. This non-parametric rank-based test was chosen over parametric alternatives because the Lilliefors test rejected normality in all four groups ($p < 0.05$ in all cases), and the Levene test indicated heterogeneity of variances across groups ($p = 0.0005$). The test revealed a highly significant difference in mean speed across subgroups ($p = 3.8 \times 10^{-30}$, Figure 4). Post-hoc pairwise comparisons using Dunn's test with Bonferroni correction confirmed significant differences between all group pairs ($p < 0.001$), with the exception of Cluster 1 vs. Cluster two ($p = 1.000$). This result is particularly informative: the two directional clusters share comparable speed profiles but differ in orientation,

10.3389/fphbi.2026.1800988

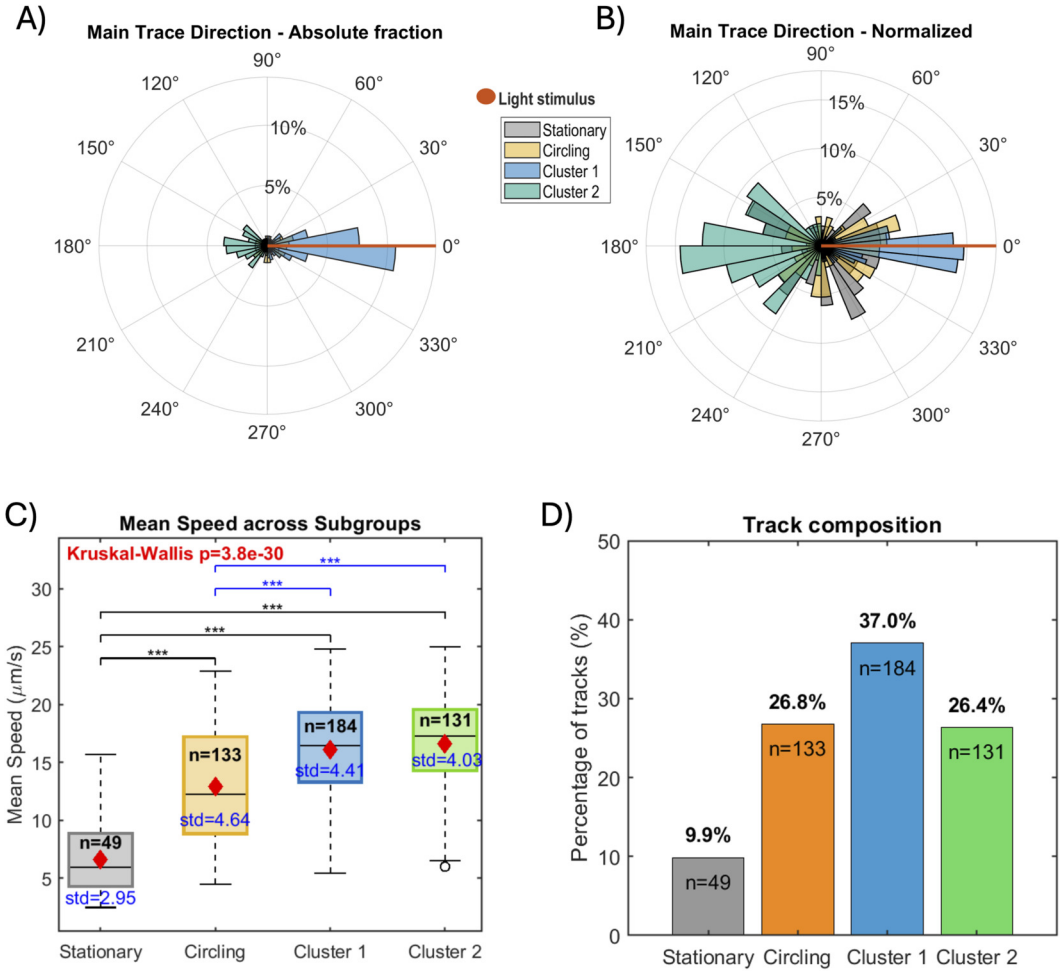

FIGURE 4
Behavioural classification and quantification of subgroups. K-means clustering was applied to the directional subgroup, partitioning it into two subpopulations with opposite phototactic responses (Cluster 1: negative phototaxis; Cluster 2: positive phototaxis). **(A)** Average angular distribution of trajectories for each behavioural group as a fraction of the total population, and **(B)** within-group normalised distribution, in which each group's angular histogram is rescaled to its own total (such that each group sums to 1), allowing comparison of directional preferences independently of group size. Both directional clusters show a clear orientation along the light source propagation axis, revealing positive or negative phototaxis depending on the group's orientation. **(C)** Comparison of mean swimming speed across subpopulations. Stationary cells show markedly lower speeds than all motile subgroups. A Kruskal–Wallis test revealed a significant overall difference ($p = 3.8 \times 10^{-30}$); post-hoc pairwise comparisons using Dunn's test with Bonferroni correction confirmed significant differences between all group pairs ($p < 0.001$), except between Cluster one and Cluster two ($p = 1.000$), which share comparable speed profiles while differing in orientation. The *n* values correspond to the number of trajectories classified in each kinematic subgroup. **(D)** Percentage composition of the population across the four behavioural groups: stationary, confined/circling, and directional (Cluster one and Cluster 2), where *n* values correspond to the number of trajectories classified in each kinematic subgroup.

confirming that the k-means segmentation captures directional information rather than a kinematic artefact.

In the case of directional trajectories, clustering isolates two kinematically coherent populations: one characterised by negative phototaxis (Cluster 1) and one by positive phototaxis (Cluster 2). The results shown in Figure 4 demonstrate how the division into four subpopulations allows distinct and consistent behaviours to emerge, including the directional and spatial coherence of collective phototactic movement and the internal consistency of kinematic parameters within each subgroup. A reflection of the characteristic motility that defines each behavioural class.

Comparison with the global population confirms that the directional subpopulations, although representing only a fraction of the total sample, account for the dominant contribution to the overall phototactic response. Figure 5 shows the kinematic data for Cluster 1.

4.3 Temporal dynamics and mean square displacement (MSD)

Mean square displacement (MSD) is a key indicator of cell diffusion dynamics. Analysis of MSD across the entire experiment and individual trajectories reveals substantial differences in the diffusion regime of subpopulations. Data from the various fitting models for the global sample and subpopulations are reported in full in the Supplementary Material. Here, we limit discussion to the Power-Law model (Table 5). This model was chosen because it is the most suitable solution for the overall sample and mobile

10.3389/fphbi.2026.1800988

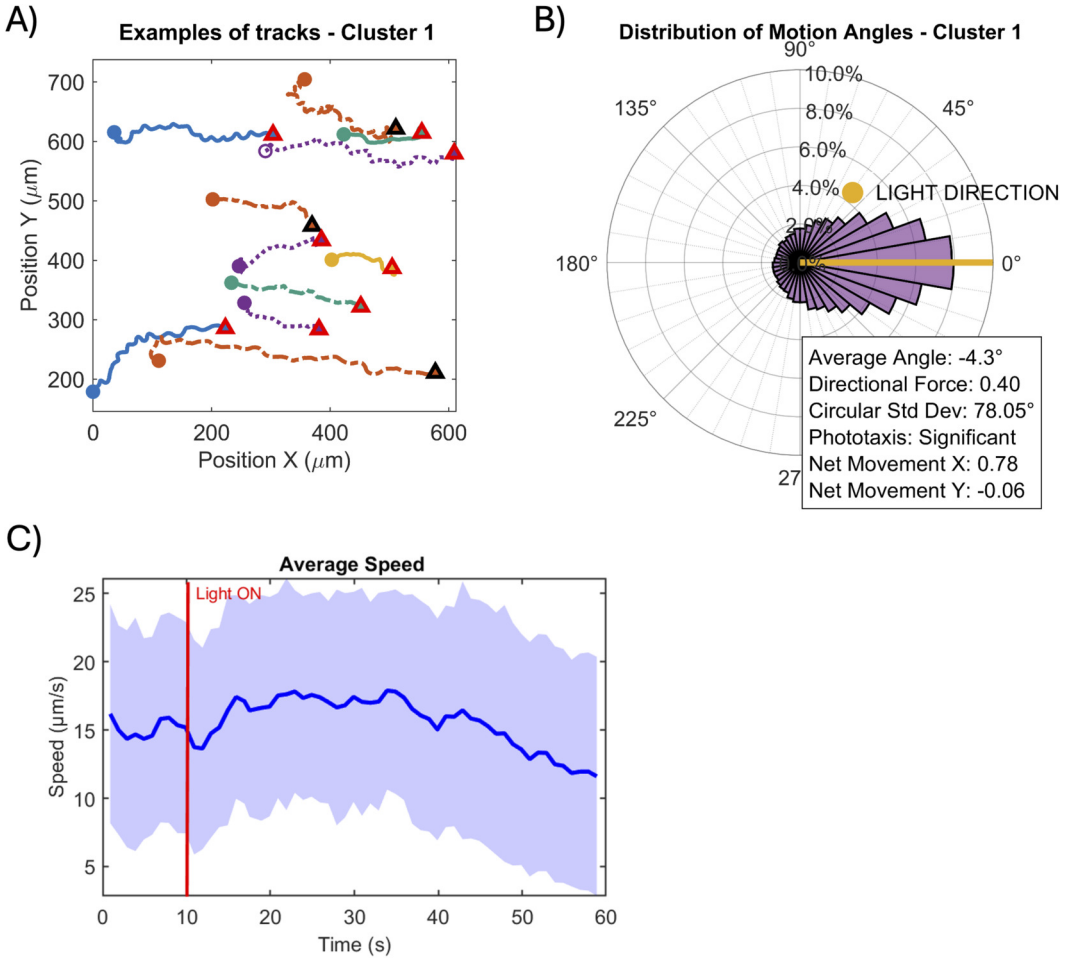

FIGURE 5
Kinematic characterisation of the subgroup with negative phototaxis (Cluster 1). **(A)** Example of raw cell trajectories traced in the presence of negative phototaxis. The starting point of the trajectory is marked by a dot, the end by triangle. The uniformity of orientation and spatial coherence confirms the directional nature of the cluster. **(B)** Distribution of movement angles. A dominant peak aligned with the light source is clearly visible, confirming the presence of negative phototaxis and demonstrating that the preferred direction only becomes evident after segmentation into subpopulations. **(C)** Average speed over time. The time trend highlights the dynamics of the motor response to the activation of the light stimulus at 10 s and shows the kinematic coherence within the group.

TABLE 6 **Power Law model parameters for mean square displacement (MSD).**

Power-law model: b parameter	Value	Error	R2	RMSE
Global (all tracks)	1.94	0.03	0.9997	3.35
Stationary	1.63	0.06	0.9977	0.77
All motile				
Circling	1.84	0.03	0.9995	2.99
Cluster 1	1.96	0.03	0.9997	4.30
Cluster 2	1.98	0.03	0.9998	3.85

For each group, the coefficient b, standard error, determination coefficient (R^2) and RMSE, obtained as average values over time are reported. The value of b quantifies the diffusion regime and distinguishes between confined (b < 1), normally diffusive (b = 1) and superdiffusive/directional (b > 1) motion. The data relate to the global, the confined and motile subpopulations (including all subgroups with motility) and those relating to the circling subgroup, Cluster one and Cluster 2. Note that the low RMSE, of the stationary subgroup reflects the small absolute MSD, values of confined trajectories rather than a superior model fit; the estimated b = 1.63 is higher than expected for genuinely confined motion, a known artefact of power-law fitting in the absence of a true diffusive plateau. This subgroup is included for completeness and cross-group comparability. On the other hand, a clear gradient can be observed: b increases from stationary → circling → global → cluster 1 ≈ cluster 2 ≈ 2.

10.3389/fphbi.2026.1800988

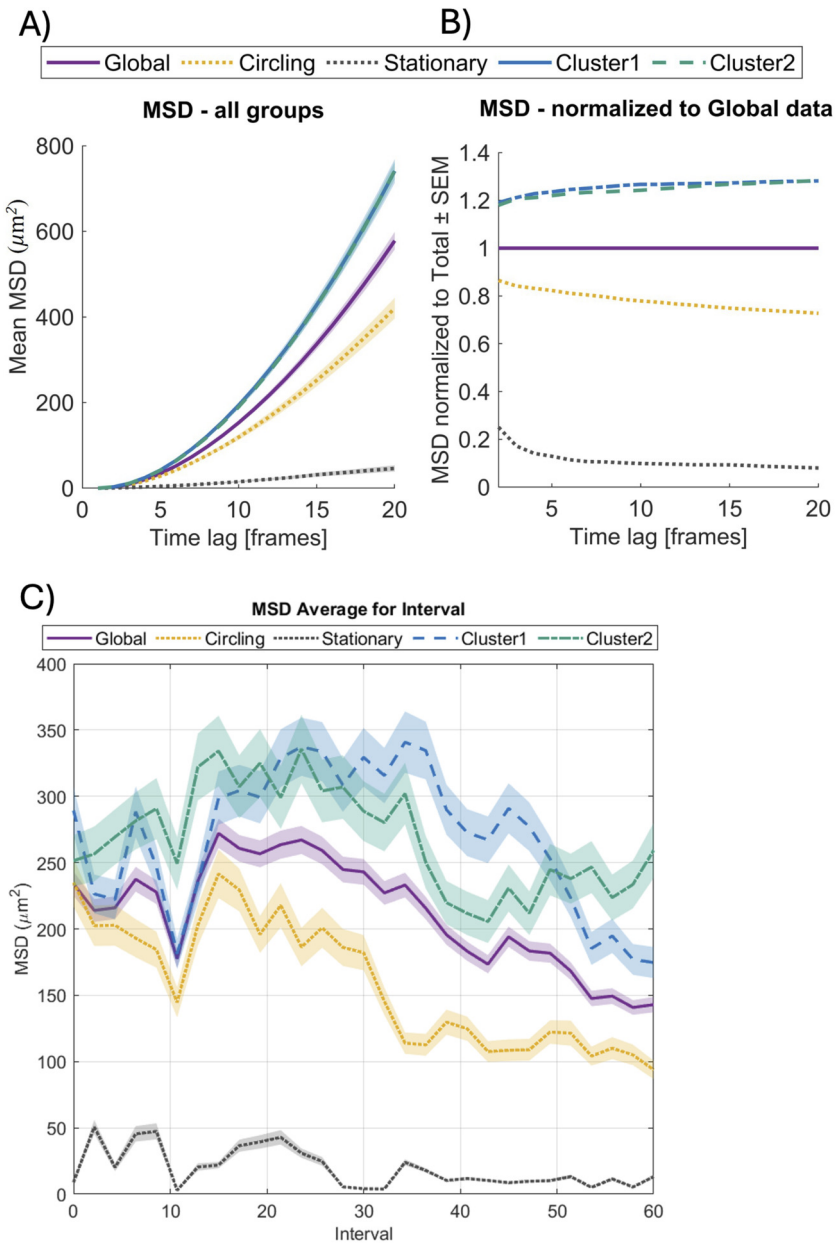

FIGURE 6
Comparison between MSD for population and subgroups. Panels **(A,B)** show the average MSD curves for the entire experiment (60 s). Panel **(A)** shows the raw curves: the model that best fits the experimental data of motile cells is the Power-Law, as shown by the exponential trend of the curves. Therefore, the resulting motion can be classified as superdiffusive, confirming what was observed experimentally. Panel **(B)** shows the same curves normalised with respect to the curve of the entire (global) population. This trend highlights the increase in superdiffusive regimes of phototactic clusters and the subdiffusive regime of the stationary subgroup. Panel **(C)** shows the variation of the average absolute value of the MSD over time during the experiment. It is clear that the stationary subgroup has a much lower MSD than the motile groups, confirming the kinetic data; the clusters have more positive values than the cells that move in a confined/circling motion, demonstrating that the MSD is also able to characterise the coherence of the motion. Shaded areas in all panels represent the standard error of the mean (SEM) computed across individual algal trajectories. Note that the MSD analysis operates only on complete trajectories within each non-overlapping time window; the number of trajectories contributing to each window is therefore a subset of the total n of the subgroup.

subpopulations. It is noisy only for the stationary subgroup, where parameter adaptation can be unstable because it is effectively confined motion. Nevertheless, in order to compare the differences that emerge between subpopulations, it is necessary to refer to a unique model. The Power-Law model allows us to quantify differences in diffusion regimes through the anomalous diffusion exponent b (where b < 1 indicates subdiffusion, b = 1 normal diffusion, and b > 1 superdiffusion consistent with persistent active motion; see Table 5). The circling and stationary subgroups show lower b values than the phototactic clusters, which stabilise around b ≈ 2, indicative of superdiffusive and highly coherent motion. Table 6 reports the mean values of b, R^2 and RMSE for each subgroup.

Figure 6 shows the MSD data and highlights these aspects more clearly: the MSD curves of the phototactic clusters show higher increases than the others, and normalisation with respect to the global population allows the dominance of the directional clusters to be visualised; the map of parameters a and b allows for immediate comparison of the dynamic regimes of the different groups, and the temporal dynamics of the mean value show both the range of motility and the presence of a reaction to the stimulus. These results demonstrate the method's ability to capture intra-population dynamic variability, showing how each subgroup contributes to the overall behaviour. The individual analyses of the subgroups are presented in the SI.

4.4 Biological and methodological considerations

The results demonstrate that the proposed method is capable of automatically identifying, within a mixed population of microswimmers, kinematically coherent subpopulations. The method allows not only for robust classification of different behaviours, but also for quantification of their contribution to the collective response induced by an external stimulus, such as light.

The analysis is independent from the molecular origin of the response and can be strengthened by orthogonal biological controls enabled by the genetic tractability of *C. reinhardtii*. For example, phototaxis-impaired or photoreceptor/signalling mutants can be analysed within the same workflow to verify the expected loss (or inversion) of stimulus-aligned directionality and to benchmark segmentation/clustering performance against a known negative-control phenotype. While such mutant validation is beyond the scope of the present demonstration, the method is designed to support these comparisons directly under matched imaging and stimulation conditions.

From a biological point of view, the ability to distinguish subpopulations with opposite reactions to a stimulus or different modes of motility offers a substantial advantage in the study of intra-population variability, an aspect rarely explored in the literature on phototaxis.

From a methodological point of view, the proposed workflow is extremely flexible and generalisable: it is based on open-source software (TrackMate (Ersho et al., 2022)) and allows scalable analysis of hundreds of trajectories. It is applicable to other biological or synthetic microswimmers, different stimulation patterns and variable experimental contexts. The combined efficiency of segmentation, clustering, and MSD analysis makes the method a powerful quantitative approach for studying emerging behaviour in populations of microscopic swimmers.

5 Discussion

In this study, we developed and validated an integrated quantitative approach for analysing motility in active particle systems, using populations of *C. reinhardtii* as an application example. The method combines segmentation and clustering based on robust kinematic parameters to map and subdivide the sample into subpopulations expressing the same type of motility, mean squared displacement analysis on time windows with multi-model fitting of dynamic regimes, and evaluation of mobility changes over time.

This analytical framework allows us to overcome the limitations of traditional methods, which typically rely on global averages or overall MSD, completely losing the internal dynamic structure of the population.

The main contribution of this work is the demonstration that the motility of active systems cannot be understood through a single aggregate measure but requires the decomposition of behaviour into coherent kinematic components. Our method allows us to identify and quantify subpopulations with distinct dynamic regimes (persistent, circling, confined, stationary) and to follow their evolution over time in response to external stimuli. This capacity for "behavioural resolution" cannot be achieved with global approaches available in the literature, either through average MSD or through static dynamic models.

The introduction of multi-model fitting (including free diffusion, ballistic motions, anomalous diffusion, exponential models, and the Ornstein–Uhlenbeck process) allows for a more precise characterisation of dynamic regimes than commonly used single models. Window analysis also allows the detection of dynamic transitions that would remain invisible in global MSD, filling a significant gap in the literature on microbial motility and active systems.

From a biological perspective, the method provides a quantitative and interpretable description of the behaviour of heterogeneous populations. It allows the response of dynamically distinct subgroups within the same sample to be separated and identifies which components drive the collective response to a stimulus, revealing subtle but significant variations in mobility that escape traditional aggregate metrics. This offers deeper insight into the mechanisms underlying phototaxis and, more generally, active orientation processes.

Finally, the approach is applicable to a wide range of organisms and systems, providing a robust framework for analysing and comparing complex dynamics under different experimental conditions, contributing significantly to the development of quantitative methods for active particle biology.

Data availability statement

The original contributions presented in the study (datasets and code) are freely available at this DOIs: 10.5281/zenodo.19354253; 10.5281/zenodo.19364857.

Author contributions

AB: Conceptualization, Data curation, Formal Analysis, Methodology, Software, Writing – original draft. AP: Investigation, Supervision, Writing – review and editing. GP: Conceptualization, Funding acquisition, Supervision, Writing – review and editing.

Funding

The author(s) declared that financial support was received for this work and/or its publication. This work is co-funded by the

European Union (ERC, EOS, 101115925). Views and opinions expressed are however those of the author(s) only and do not necessarily reflect those of the European Union or the European Research Council. Neither the European Union nor the granting authority can be held responsible for them.

Conflict of interest

The author(s) declared that this work was conducted in the absence of any commercial or financial relationships that could be construed as a potential conflict of interest.

The author GP declared that they were an editorial board member of Frontiers at the time of submission. This had no impact on the peer review process and the final decision.

Generative AI statement

The author(s) declared that generative AI was used in the creation of this manuscript. Generative AI was used only for proofreading (spelling, grammar, and minor clarity edits).

Any alternative text (alt text) provided alongside figures in this article has been generated by Frontiers with the support of artificial intelligence and reasonable efforts have been made to ensure accuracy, including review by the authors wherever possible. If you identify any issues, please contact us.

Publisher's note

Supplementary material

The Supplementary Material for this article can be found online at: https://www.frontiersin.org/articles/10.3389/fphbi.2026.1800988/full#supplementary-material

References

Arrieta, J., Barreira, A., Chioccioli, M., Polin, M., and Tuval, I. (2017). Phototaxis beyond turning: persistent accumulation and response acclimation of the microalga Chlamydomonas reinhardtii. *Sci. Rep.* 7, 3447. doi:10.1038/s41598-017-03618-8

Berg, H. C. (1993). *Random Walks in Biology*. Princeton University Press.

Chau, R. M. W., Ursell, T., Wang, S., Huang, K. C., and Bhaya, D. (2015). Maintenance of motility bias during cyanobacterial phototaxis. *Biophys. J.* 108, 1623–1632. doi:10.1016/j.bpj.2015.01.042

Choudhary, S. K., Baskaran, A., and Sharma, P. (2019). Reentrant efficiency of phototaxis in *Chlamydomonas reinhardtii* cells. *Biophys. J.* 117, 1508–1513. doi:10.1016/j.bpj.2019.09.016

Colabrese, S., Gustavsson, K., Celani, A., and Biferale, L. (2025). Flow navigation by smart microswimmers *via* reinforcement learning. *Phys. Rev. Lett.* 118, 158004. Available online at: https://journals.aps.org/prl/abstract/10.1103/PhysRevLett.118.158004.

Drescher, K., Goldstein, R. E., and Tuval, I. (2010). Fidelity of adaptive phototaxis. *Proc. Natl. Acad. Sci.* 107, 11171–11176. doi:10.1073/pnas.1000901107

Ershov, D., Phan, M. S., Pylvänäinen, J. W., Rigaud, S. U., Le Blanc, L., Charles-Orszag, A., et al. (2022). TrackMate 7: integrating state-of-the-art segmentation algorithms into tracking pipelines. *Nat. Methods* 19, 829–832. doi:10.1038/s41592-022-01507-1

Feinleib, M. E. H., and Curry, G. M. (1971). The relationship between stimulus intensity and oriented phototactic response (Topotaxis) in chlamydomonas. *Physiol. Plant.* 25, 346–352. doi:10.1111/j.1399-3054.1971.tb01453.x

Fisher, N. I. (1995). *Statistical Analysis of Circular Data*. Cambridge University Press.

Ghezzi, A., Lenz, A. J. M., Soldevila, F., Tajahuerce, E., Vurro, V., Bassi, A., et al. (2023). Computational based time-resolved multispectral fluorescence microscopy. *Apl. Photonics* 8, 046110. doi:10.1063/5.0135452

Gorman, D. S., and Levine, R. P. (1965). Cytochrome f and plastocyanin: their sequence in the photosynthetic electron transport chain of Chlamydomonas reinhardi. *Proc. Natl. Acad. Sci.* 54, 1665–1669. doi:10.1073/pnas.54.6.1665

Irimia, D. (2010). Microfluidic technologies for temporal perturbations of chemotaxis. *Annu. Rev. Biomed. Eng.* 12, 259–284. doi:10.1146/annurev-bioeng-070909-105241

Korobkova, E., Emonet, T., Vilar, J. M. G., Shimizu, T. S., and Cluzel, P. (2004). From molecular noise to behavioural variability in a single bacterium. *Nature* 428, 574–578. doi:10.1038/nature02404

Leptos, K. C., Wan, K. Y., Polin, M., Tuval, I., Pesci, A. I., and Goldstein, R. E. (2013). Antiphase synchronization in a flagellar-dominance mutant of chlamydomonas. *Phys. Rev. Lett.* 111, 158101. doi:10.1103/PhysRevLett.111.158101

Morel-Laurens, N. (1987). Calcium control of phototactic orientation in chlamydomonas reinhardtii: sign and strength of response. *Photochem. Photobiol.* 45, 119–128. doi:10.1111/j.1751-1097.1987.tb08412.x

Oral, C. M., Ussia, M., and Pumera, M. (2022). Hybrid Enzymatic/Photocatalytic degradation of antibiotics *via* morphologically programmable light-driven ZnO microrobots. *Small* 18, 2202600. doi:10.1002/smll.202202600

Orozco, J., Jurado-Sánchez, B., Wagner, G., Gao, W., Vazquez-Duhalt, R., Sattayasamitsathit, S., et al. (2014). Bubble-Propelled micromotors for enhanced transport of passive tracers. *Langmuir* 30, 5082–5087. doi:10.1021/la500819r

Polin, M., Tuval, I., Drescher, K., Gollub, J. P., and Goldstein, R. E. (2009). Chlamydomonas swims with two "Gears" in a eukaryotic version of run-and-tumble locomotion. *Science* 325, 487–490. doi:10.1126/science.1172667

Qian, H., Sheetz, M. P., and Elson, E. L. (1991). Single particle tracking. Analysis of diffusion and flow in two-dimensional systems. *Biophys. J.* 60, 910–921. doi:10.1016/S0006-3495(91)82125-7

Sagawa, T., Kikuchi, Y., Inoue, Y., Takahashi, H., Muraoka, T., Kinbara, K., et al. (2014). Single-Cell E. coli response to an instantaneously applied chemotactic signal. *Biophys. J.* 107, 730–739. doi:10.1016/j.bpj.2014.06.017

Schneider, C. A., Rasband, W. S., and Eliceiri, K. W. (2012). NIH Image to ImageJ: 25 years of image analysis. *Nat. Methods* 9, 671–675. doi:10.1038/nmeth.2089

The MathWorks Inc. MATLAB (2022). *Version: 9.13.0 (R2022B)*. Natick, Massachusetts: The MathWorks Inc.

Till, S., Ebmeier, F., Fragkopoulos, A. A., Mazza, M. G., and Bäumchen, O. (2022). Motility and self-organization of gliding Chlamydomonas populations. *Phys. Rev. Res.* 4, L042046. doi:10.1103/physrevresearch.4.l042046

Tsang, A. C. H., and Riedel-Kruse, I. H. (2024). Light-dependent switching between two flagellar beating states selects versatile phototaxis strategies in microswimmers. *Proc. Natl. Acad. Sci.* 121, e2408082121. doi:10.1073/pnas.2408082121

Urso, M., Ussia, M., and Pumera, M. (2021). Breaking polymer chains with self-propelled light-controlled navigable hematite microrobots. *Adv. Funct. Mater.* 31, 2101510. doi:10.1002/adfm.202101510

Varuni, P., Menon, S. N., and Menon, G. I. (2017). Phototaxis as a collective phenomenon in cyanobacterial colonies. *Sci. Rep.* 7, 17799. doi:10.1038/s41598-017-18160-w

Wakabayashi, K., Misawa, Y., Mochiji, S., and Kamiya, R. (2011). Reduction-oxidation poise regulates the sign of phototaxis in Chlamydomonas reinhardtii. *Proc. Natl. Acad. Sci.* 108, 11280–11284. doi:10.1073/pnas.1100592108

Wang, Z., and Tsang, A. C. H. (2025). Intermediate light adaptation induces oscillatory phototaxis switching and pattern formation in *Chlamydomonas*. *Proc. Natl. Acad. Sci.* 122, e2425369122. doi:10.1073/pnas.2425369122

Wu, X.-L., and Libchaber, A. (2000). Particle diffusion in a quasi-two-dimensional bacterial Bath. *Phys. Rev. Lett.* 84, 3017–3020. doi:10.1103/PhysRevLett.84.3017